Optimized Design and Multiphysics Analysis of a Ka-Band Stacked Antenna for CubeSat Applications

Marco Simone ⓘ, Matteo Bruno Lodi ⓘ, *Graduate Student Member, IEEE*, Nicola Curreli ⓘ,
Santi Concetto Pavone ⓘ, *Senior Member, IEEE*, Giuseppe Mazzarella ⓘ, *Senior Member, IEEE*,
and Alessandro Fanti ⓘ, *Member, IEEE*

Abstract—Nowadays, the use of CubeSats for telecommunications and interplanetary missions is ever-increasing, thanks to their appealing low-cost character, as well as the space environment, which poses challenging multiphysics constraints on the antenna design. In this framework, the use of Ka-band for communication is explored. We present the design of a stacked patch antenna working across the down- and uplink Ka-bands. Materials and geometry of the radiator have been selected by accounting for the trade-off between electromagnetic, thermal and mechanical requirements. The design of the antenna is performed with a particle swarm optimization algorithm developed to control the bandwidth and matching. A bandwidth of 5.53@33.185 GHz has been obtained, with a gain around 8 dB. Furthermore, a multiphysics thermal analysis is performed to verify the operational stability of the optimized array, mounted on a 1 U satellite, in a case-study mission. The temperature patterns in the array are evaluated during the orbital period, and the influence of the operative temperature on the antenna responses and gain was considered. We found that the thermal loads can affect the antenna matching. However, thanks to the optimized design, the proposed stacked antenna can operate from $-100\,°C$ to $100\,°C$, with an almost constant gain. Finally, following a damage-tolerant approach, the level of mechanical deformation, which could be induced on the communication system, was studied. The stress analysis reveals that the stacked geometry can be used in a space mission. From the investigation of the strain and displacement field, we found a negligible impact on the antenna performance.

Index Terms—CubeSat, multiphysics, particle swarm optimization, stacked antenna, thermal stresses, Ka-band.

Marco Simone, Matteo Bruno Lodi, Giuseppe Mazzarella, and Alessandro Fanti are with the Department of Electrical and Electronic Engineering, University of Cagliari, Cagliari 09123, Italy (e-mail: marco.simone.84@gmail.com; matteobrunolodi@ieee.org; mazzarella@unica.it; alessandro.fanti@diee.unica.it).

Nicola Curreli is with the Istituto Italiano di Tecnologia (IIT), Genoa 16163, Italy (e-mail: nicola.curreli@iit.it).

Santi Concetto Pavone is with the Department of Electrical, Electronics, and Computer Engineering (DIEEI), University of Catania, Catania 95125, Italy (e-mail: santi.pavone@unict.it).

I. INTRODUCTION

CUBESATS are low-cost, cube-shaped (10 cm × 10 cm × 10 cm) nano-satellites (1–10 kg) used for remote sensing, telecommunications, deep-space communications and interplanetary missions [1]–[6]. Despite being firstly conceived for educational purposes, the cost-effective features of CubeSats led to the wide adoption of these spacecraft systems [1], [2], [4]. In the last years, the interest in CubeSat has expanded: Low Earth Orbit (LEO), higher orbits for Earth Science Missions (ESM), or deep space communications are applications increasingly studied [6], [7]. In this framework, new and effective communication systems are needed. As a result, the trend in CubeSat antennas is to move from the S-band (2–4 GHz) to the X-band (8–8.4 GHz) and Ka-band (26–34.7 GHz for down- and uplink) [6], [8]. Ka-band antennas are at an early-stage technology, but some devices are under development, such as the ≃1 kg horn-based systems Landmapper, with 300 Mbps downlink transmitter (Astro Digital) [9]. However, the Technology Readiness Level (TRL) is still relatively low. Therefore, it is necessary to push the forefront towards new engineering solutions [9].

Few K/Ka-band antenna designs have been proposed for CubeSat deep space missions [6]. A phased 8 × 8 circularly polarized array of microstrip patches, with 1.5 GHz bandwidth, was proposed [10]. Antenna array technology for CubeSat is interesting and promising since it ensures compactness, while enabling beamforming [10], [11]. The beamforming and the steering can increase the exploration margin up to ±40°, relative to the broadside direction, which is useful in the case of unknown constellation status [6]. Recently, in [12], the electromagnetic design, driven by volume and weight constraints, as well as mechanical choices, resulted in the high-gain (42 dBi) KapDA mesh reflector, working at about 33 GHz, mounted on a 6 U CubeSat [13]. An additively manufactured metallic metasurface antenna, with a 26.1 dB gain, was designed at 32 GHz for space applications [14]. Chahat *et al.* designed and tested, on a 12 U CubeSat, the 1 m KaTENna mesh reflector working at 36 GHz, reporting a 48.4 dBic gain, with a 62% efficiency [5], [11]. A summary of the most relevant and recent Ka-band antennas for CubeSat is reported in Table I.

For any communication system to be mounted on a nano-satellite platform, low mass (maximum 50 g), reduced thickness (maximum 5 mm), and small size (maximum 90 mm × 90 mm) are required [15]. Modularity is another factor to be taken into

TABLE I
KA-BAND ANTENNAS FOR CUBESAT

Ref.		Freq. (GHz)	BW (GHz)	Gain (dBi)	Efficiency (%)	Size (mm^2)	Weight (g)	Optimized	Multiphysics Analysis
[10]	Patch	37	1.5	24.04	-	90.2 x 90.2	$\sim$50	Y	N
[7]	Horn + Mesh Reflector	33	$\simeq$1	42.6	57	100 x 100	150	Y	N
[5]	Horn + Mesh Reflector	32	5	50	58	100 x 100	-	Y	N
[14]	Metasurface	32	5	26.1	40	13 x 13	-	Y	N
This work	Stacked Patch	32, 34.5	5.53	26	97.5	49 x 49	25	Y	Y

account [11]. The antenna should be easily deployable, with no failure risks, and attached to the external spacecraft surface [11], [15]. Furthermore, from an antenna engineering point of view, high gain (>25 dBi), operational bandwidth (BW), duplex mode operations, and (right-hand) circular polarization (CP) have been identified as the most critical aspects for CubeSats applications [6]. Indeed, medium to high-gain (12 dBi, >25 dBi) [11] and CP are features to limit signal attenuation and polarization mismatch [10], [16]. A CubeSat communication module must allow the communication for a maximum of 2 km, *i.e.*, the typical separation distance in formation-flying missions [6]. From the analysis of the state-of-the-art (Table I), the system communication requirements translate into the frequent design and application of antennas such as horns [17], deployable reflectors [8], and reflectarray (e.g., that used in the LEO ISARA mission) [18]. The best antenna design cannot be easily selected [6]. Indeed, despite mesh reflectors allow to obtain a high gain value, they are usually bulky and the mechanical issues cannot be underestimated [12]. Similarly, although horn antennas are generally compact and achieve satisfactory communication performances, they keep an issue in terms of size and, therefore, weight. As a result, there is room for designing a CubeSat antenna working at Ka-band, which could satisfy the aforementioned criteria. Stacked patch antennas stood out as promising candidates being lightweight, and since they can reach high gain in array configuration, while allowing beam steering capability [19].

Stringent and precise design requirements for the communications subsystem must be considered in the design [6], [11]. However, the physical specifications for the spacecraft and its sub-systems cannot be neglected. The mechanical and thermal environments that the satellite antenna must face in outer space are very complicated and harsh [1], [4], [11]. For instance, the antenna must be manufactured with materials that comply with mechanical and thermal constraints of space missions [11]. Issues like mechanical degradation due to cosmic high-energy radiation or electrostatic discharge and dielectric breakdown must be considered when choosing the materials and the antenna topology [6], [11]. As a result, from the analysis of the state-of-the-art (Table I), very few works present a multiphysics analysis of an antenna or an array to study or demonstrate the compliance to mechano-thermal constraints and the safety of the spacecraft during operations. For instance, the natural frequencies of an ultra high frequency loop antenna were investigated by finite element analysis (FEA), or the spectrum of acceleration on a reflector antenna, mounted on 1.5 U CubeSat, was studied [11].

The thermal aspects and stresses induced in CubeSat antennas during the operation are underestimated. Thermal analysis (TA) is a major engineering work in the development process of satellite components and systems [20]–[22]. Thermal analysis is useful for the design and verification stages [20]. The operational conditions of batteries, printed circuit boards (PCB), and solar cells are studied for the worst hot and cold cases [21]. In this framework, theoretical analysis, commercial software, or complex numerical algorithms have been developed [20]–[22]. For instance, by direct integration of linearized, second-order differential equation model was treated to provide a single-node approximation of the temperature evolution during the orbits [20]. On the other hand, spreadsheet-based commercial software is available [23], and dedicated FEA programs, such as Systema Thermica [24], were developed [22]. In addition, the Monte Carlo ray-tracing method was used for simulating the temperature dynamics in space [23]. The analytical approach to the thermal analysis, the complex, multiphysics and non-linear nature of the physical scenario hampers the feasibility of finding closed-form solutions under realistic operating conditions. Therefore, numerical analysis is required for TA.

In this paper, the design and optimization of a Ka-band antenna, for down- and uplink operations, which serves as an efficient communication system in the space environment, is proposed. We demonstrate that the multiphysics study on the influence of antenna geometry and materials on thermal deformation and stresses is effective and allows to meet the requirements and constraints imposed by CubeSat missions.

The paper is organized as it follows. In Section II the antenna geometry is presented, together with the considerations on architecture and materials in relation to satellite application. Section III discusses the electromagnetic optimization of the antenna geometry. Section IV discloses the framework of mathematical equations which represent the multiphysics model used to evaluate the conformity of the antenna to CubeSat applications. The temperature evolution during a case-study LEO mission is simulated, and the thermal stresses induced in the system are investigated. In Section V the results of the analysis are presented. Finally, the conclusions on the proposed design are drawn.

II. ANTENNA DESIGN

A. Geometry of the Radiating Element

The proposed antenna aims to obtain both a wideband operation at Ka-band and gain higher than the traditional patch
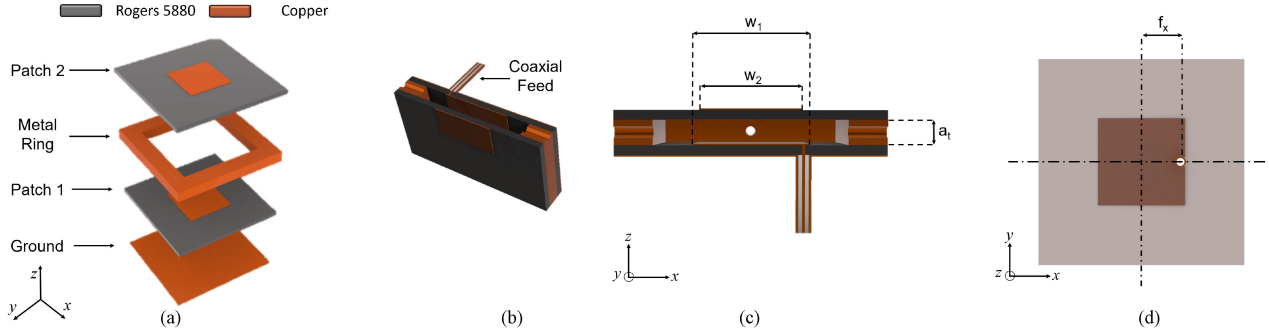
Fig. 1. Antenna geometry: (a) 3D layout of the stacked patch antenna made in Rogers RT/duroid 5880 and copper. Rogers RT/duroid 5880 is characterized by low losses at Ka-band, relatively low cost, while being approved for space applications, given its good thermal and mechanical properties (as studied in Section V-C). (b) View to show where the small hole for eventual outgassing and pressure management can be opened. (c) Side view with details of the geometry variables to be optimized (the width of the lower and upper patch, *i.e.,* w_1 and w_2 respectively, and the air gap a_t. (d) Bottom view for the vposition of the coaxial feed f_x.

antennas of comparable physical dimensions [10]. The wide frequency band allows using the same antenna for down- and uplink bands [11], [14]. This is a non-trivial achievement and cannot be obtained by using a single-layer patch antenna. At the same time, the higher gain of the single radiating element reduces the number of antennas required to obtain the desired array antenna gain, thus improving also the final radiation efficiency.

The antenna geometry is summarized in Fig. 1. It consists of a stack of two patches supported by two Rogers RT/duroid 5880 substrates [25], 0.254 mm thick, separated by an air gap (a_t thick) and sustained by a metallic ring (Fig. 1(a) and Fig. 1(c)). The lower substrate is ground-backed (Fig. 1(a)). We made use of this configuration because of its very compact format. At the same time, thanks to the coupling of the resonances given by the two patches, a bandwidth enhancement is achieved [19], [26]–[30]. Stacked patch antennas were proposed in [19] for LEO communications, but they also find application in various fields encompassing both 5G antenna arrays [31] and reflectarrays [32], in which the requirements push to an antenna that has to be both low-profile and inherently wideband. Rogers RT/duroid 5880 is widely used at these frequencies, because of its reasonable losses at Ka down- and uplink bands, while presenting suitable thermal, mechanical properties [25], which have been analysed and presented in the Sections V-C and V-D related to our particular proposed geometry, whose air gap under the upper laminate could lead to undesired deformations. These characteristics lead to the approval of this substrate for space applications. Its mechanical suitability is confirmed by other Cube-Sat antennas proposed in literature operating in other frequency bands, as the patch antenna proposed in [33] (see Fig. 3 in [33]).

The metallic patches and the air gaps present squared shapes, which allow dual linear or circular polarization. The air gap width is set to 5 mm, close to half-wavelength at 33 GHz. The feeding system consists of a feeding point (Fig. 1(b) and Fig. 1(d)), centered on an axis and shifted towards the orthogonal edge. The single element operating principles are based on the coupled resonances of the two patches. The upper parasitic patch acts as a double layer (RT/duroid 5880 and air) substrate-based patch antenna, whereas the lower patch can be considered the ground of the upper one. The air gap reduces the energy stored

below the patch, and therefore leads to a larger bandwidth [27]–[30]. Moreover, the parasitic patch affects the normal operation of the lower one, which does not radiate in free space.

Although this complexity furthers a wideband operation, it drives the design process on a more demanding road with respect to the single-patch printed antennas. The coupling between the patches is very sensitive with respect to the geometric parameters, and this is reflected in the resonance frequencies. Therefore, the result is a non-trivial analytical model for predicting them. To maximize the performance of this antenna, which are the wide frequency band operation and the low-profile structure, it is necessary to consider all the relevant parameters to be tuned. From this, the operating frequency band maximization with respect to the geometrical parameters is the main issue in the design, and it can be reached via an optimization technique.

B. Antenna Materials and Configuration for Compliance With Spacecraft Requirements

A CubeSat antenna must be manufactured with materials that comply with mechanical and thermal constraints of space missions [6], [11]. Given the promising mechanical and communication features of the stacked patch antennas for space applications [19], [30], it is mandatory to complement the design choices by carefully selecting suitable materials. For instance, Rogers RT/duroid 6010 ($\epsilon_r = 6.15$, at room temperature) is approved for spacecraft applications, due to its coefficient of thermal expansion (CTE = 24–50 ppm/°C) and outstanding resistance to outgassing, *i.e.,* the release of gases or volatile condensable matter in vacuum [15]. The subsequent mass loss can affect the material mechanical and electrical properties [11]. However, for a given space mission both the payload and the costs of the substrates are relevant aspects [6]. In this context, the Rogers RT/duroid 5880 ($\epsilon_r = 2.2$, at 25 °C, with a variation of -125 ppm/°C, CTE = 31–237 ppm/°C) is a cheaper but tested and approved substrate for space applications [25]. We designed the stacked patch antenna working at Ka-band by using Rogers RT/duroid 5880 as substrate for both patches, and copper as conductor material ($\sigma = 5.9 \cdot 10^7$ Sm^{-1}).

The satellite application dictates that the antenna has to face more issues and respect more requirements with respect to a normal application on Earth, thus requiring a little modification in the traditional geometry [19], [30]. The out-of-atmosphere operation is an issue that can affect the performance of the stacked configurations. The presence of the air gap can deform the dielectric slab shape, so that also the impedance matching may be affected. Also, the high pressures in the take-off stage may lead to similar outcomes [34]. Therefore, a small hole (with a radius of r = 0.15 mm) can be opened at the center of each side of the metal ring to allow the air to flow outside, as shown in Fig. 1(c). The hole characteristic size is much lower than operative wavelengths (the diameter is smaller than $\lambda_0/30$), then it does not affect the electromagnetic performance of the antenna. The thermal stress close to the hole must be monitored to avoid failure or operation-related issues.

Furthermore, the proposed stacked patch antenna (Fig. 1), working both in the down- and uplink Ka-band would be manufactured by relying on standard PCB technology. Therefore, given the production guidelines (such as milling and glue usage), failure prevention through mechanical analysis is required [35], [36].

III. PARTICLE SWARM OPTIMIZATION FOR CUBESAT APPLICATIONS AT KA-BAND

From the above considerations, the goal of an antenna design with maximum operative BW calls for an optimization process to manage the geometrical parameters [37], [38].

The optimization process translates the electromagnetic issue into a mathematical problem [37], *i.e.,* the search of the minimum of a multivariable function. Since this solution must provide the best antenna in terms of performances concerning the requirements, the so-called objective or fitness function, has to be properly defined to deal with the electromagnetic problem.

The use of numerical optimization techniques is not uncommon in electromagnetics for multivariable problems [37]. When the design process must satisfy multiple contrasting requirements, a trade-off can be not trivial. Different algorithms, such as Genetic [39], Evolutionary [40], and Particle Swarm Optimization (PSO) [41] algorithms have been exploited by the electromagnetic engineering community. For instance, the optimization is widely applied in metamaterial design [39], or in antenna array, where the system depends on a very large set of parameters [40], but also in other devices where the theoretical model provides only a very approximated description [26]. In this work, the PSO algorithm was used to optimize the design of the stacked patch antenna shown in Fig. 1.

The optimization consists of two parts, namely the electromagnetic analysis and the optimization cycle itself. The latter is in charge to move the swarm, composed by Np particles, inside the solution space of dimension dim. The PSO algorithm manages a set of potential solutions, randomly initialized in the solution space, with a uniformly distributed random velocity [42]

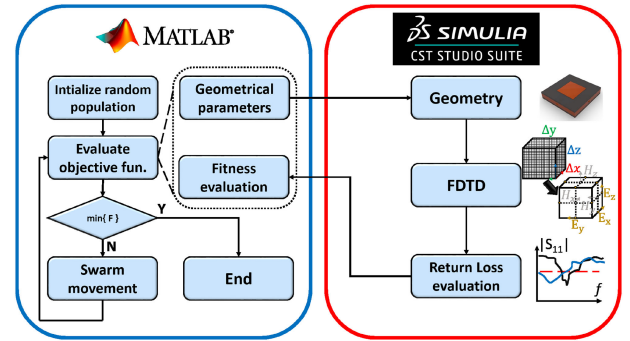$$v = 2\, r_0\, v_{\max} - v_{\max}, \tag{1}$$

Fig. 2. Summary of the PSO-based optimization algorithm for the stacked patch antenna working in Ka-band. A Matlab script initializes the Particle Swarm Optimization (PSO) parameters and passes them to CST for evaluating through the finite difference time domain (FDTD) algorithm the antennas performances. The script evaluates the fitness and iterates until the minimum of the objective function is reached.

where r_0 is a random number between 0 and 1, and updated at each iteration step according to the law

$$v_{i+1} = w \cdot v_i + c_1 \cdot r_1 \cdot (p_i - x_i) + c_2 \cdot r_2 \cdot (g_i - x_i), \tag{2}$$

$$x_{i+1} = x_i + v_{i+1}, \tag{3}$$

in order to explore the solution space and hence to find the minimum of the objective function. In (2) and (3)
- x_i is the swarm position at the ith iteration;
- v_i is the velocity which moves the swarm at the ith iteration;
- w, named inertia, tends to maintain the same movement direction;
- c_1, c_2, named acceleration constants, are two weights to encourage the movement towards the global and local minima, respectively;
- r_1, r_2 are two random numbers that perform the randomic component of the swarm movement;
- g_i and p_i are respectively the global and local minima at the iteration i.

The solution space is determined by the variables to be optimized and their variation ranges [37]. In this work, the electromagnetic analyses are carried out using CST Microwave Studio (Simulia, 3DS, GE). CST is known to offer different built-in optimization algorithms, including the PSO, but the software does not allow a full set of the algorithm. For instance, it is not possible to set all acceleration constants and it is not possible to define complex objective functions, which involve different quantities, but only their linear weighted sum. In this framework, the available software settings are limiting. Therefore, given the strict requirements and the peculiar problem at hand [19], [37], as summarized in Fig. 2, we developed an *ad hoc* PSO algorithm led by a Matlab (The MathWorks Inc., MA USA) script, which controls the PSO parameters and drives the full-wave software to evaluate the antenna performances, from which the script assesses the fitness function and manages the swarm movement.

According to the summary scheme given in Fig. 2, each set of coordinates in the solution space (*i.e.,* the position) corresponds to a possible setting of the antenna parameters to be optimized, hence the coordinates are provided from the objective function to

CST to build the antenna model and perform the finite difference time domain (FDTD) simulations to evaluate the relevant electromagnetic quantities required for the fitness computation. The figure of merit with respect to which the antenna is optimized is the Return Loss (RL), which is used as a feature to evaluate the fitness of each position for each particle at the ith iteration, and moves the population to a new set of positions according to the Eqs. (2) and (3).

The new population coordinates are the new inputs for the electromagnetic analysis in the subsequent iteration. The process iterates until particles converge to the minimum of the objective function in the solution space, *i.e.,* the optimal size of the antenna for the design requirements [6].

The solution space has been defined to contain the range to generate an antenna operating in both down- and uplink Ka-bands. The span of the solution space is an issue in the optimization problem [37]. In detail, a wider range includes a larger number of potential solutions, but at the same time this leads to a slower convergence due to the larger space to explore. Unfortunately this increases the risk of local minima, which can drive the optimization to sub-optimal solutions. Therefore, the solution space must be designed to account for the trade-off between convergence rate and the presence of optimal solution. In this framework, the number of particles has been tested and selected to minimize the risks of convergence to local minima [26]. Moreover, given the high frequency and the peculiarities of the CubeSat application involved, the solution space is constrained by the technological and manufacturing features [43]. Therefore we took into account the realistic tolerances and resolutions, thus translating the continuous solution space into a discrete one [37]. As a result, each variable is forced to assume quantized and discrete values, subject to the discretization step Δx_i. With reference to Fig. 1, the parameters involved in the optimization are

- w_1, size of the bottom patch;
- w_2, size of the upper patch;
- a_t, thickness of the air gap;
- f_x, position of the feed with respect to the patch center,

and in Table II their interval of variation is provided, thus defining the solution space. These are the geometrical parameters which mostly affect the antenna operation. The patches size w_1, w_2 play a key role in determining the resonances and therefore, the operative frequency band. The height of the air gap a_t is strongly involved in the coupling between the patches. Finally, the relative position of the feed with respect to the center of the bottom patch f_x affects the impedance matching between

TABLE II
SOLUTION SPACE

Range [mm]	Δx [mm]
$2.5 < w_1 < 3.5$	0.01
$2.5 < w_2 < 3.5$	0.01
$0.25 < a_t < 1$	0.05
$0.875 < f_x < 1.625$	0.05

the antenna and the feed, so that it is the fourth parameter to be optimized.

The positions assumed by the particles in the solution space are evaluated in terms of goodness with respect to the design requirements via the objective function, which assigns a fitness value to each position tested during the optimization. Therefore, the objective function must be defined to maximize the bandwidth (BW) with a RL better than 10 dB (10dB-BW) with a certain tolerance in the center of the frequency band with respect to the 10 dB limit. Such a function has to be designed and defined to properly evaluate all the following ambiguous cases:

- no available bandwidth;
- dual-band operation (*i.e.,* the two resonances provide two separate operative bands);
- wideband (*i.e.,* a minimum of 1 GHz) operative bandwidth;

while also driving the optimization towards the best solution. Notably, the objective function developed for optimizing the stacked patch antenna applies a combined windowing and weighting to the RL. The fitness is the sum of the resulting "shaped" RL values over the bandwidth. In mathematical terms, the weighted function $S_{11}^{wgt}(f)$ is an arc of tangent type, *i.e.,*

$$S_{11}^{wgt}(f) = \arctan\left(\frac{S_{11}(f)}{\psi}\right) \tag{4}$$

where the coefficient ψ determines the slope of the function, shown in Fig. 3, and sets the balance between the BW and the minimum RL value in the center of the frequency band, by constraining the optimization to a tolerance value for the manufacturing process. The coefficient ψ allows the proposed PSO algorithm to find an optimized solution with a desired tolerance in terms of RL value in the center of the frequency band. The window function $w(f)$, Eq. (5), shown at the bottom of this page, is a tapered cosine type (Fig. 4), where $f_{\min} = 30$ GHz, $f_{\max} = 36$ GHz and $BW_0 = f_{\max} - f_{\min}$, whilst $a = 0.4$ is the the ratio of cosine-tapered section length to the entire window length. Equation (4) is applied to the weighted function $S_{11}^{wgt}(f)$, shown in Fig. 3, to achieve a frequency band centered around

$$w(f) = \begin{cases} 0.5\left[1 + \cos\left(\pi\frac{2f}{aBW_0} - 1\right)\right] & f_{\min} \leq f \leq f_{\min} + \frac{a}{2}BW_0 \\ 1 & f_{\min} + \frac{a}{2}BW_0 < f \leq f_{\max} - \frac{a}{2}BW_0 \\ 0.5\left[1 + \cos\left(\pi\frac{2f}{aBW_0} - 1 + \frac{2}{a}\right)\right] & f_{\max} - \frac{a}{2}BW_0 < f \leq f_{\max} \end{cases} \tag{5}$$
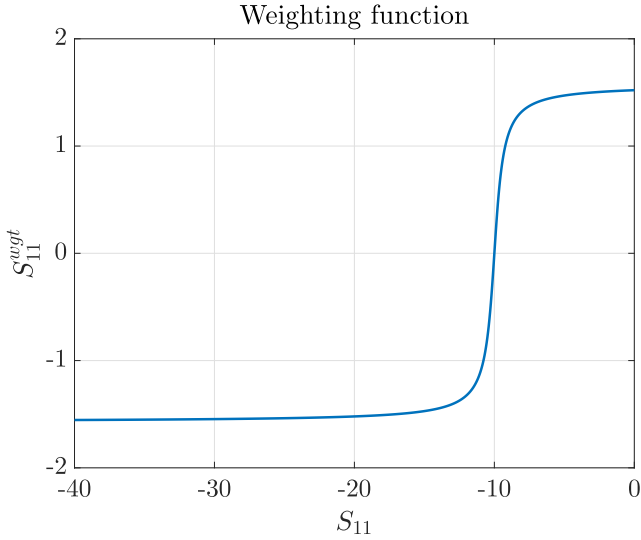
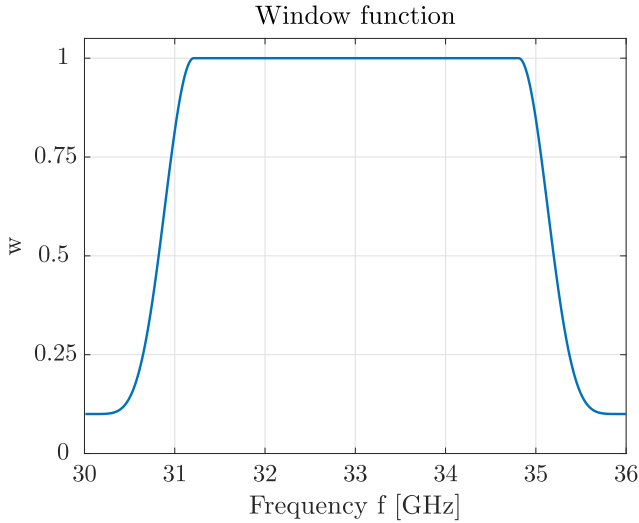Fig. 3.   Weighting function, $S_{11}^{wgt}(f)$, for $\psi = 0.5$, vs. S_{11}.

Fig. 4.   Window function, $w(f)$, over the Ka-band.

33 GHz, so that

$$S_{11}^{win}(f) = S_{11}^{wgt}(f)w(f). \tag{6}$$

The final objective function F is given by the sum of the $S_{11}^{win}(f)$ values over the whole frequency band $(f_{\min}, f_{\max})$

$$F = \sum_{f_{\min}}^{f_{\max}} S_{11}^{win}(f) \tag{7}$$

The PSO has been set with $Np = 10$ particles (2.5 times the number of variables to be optimized), acceleration constants $c_1, c_2 = 2$, and absorbing boundary conditions.

The application of a full-wave analysis technique, combined with the proposed iterative optimization algorithm, requires a long time to complete all the required simulations. Nevertheless, the discrete solution space allows reducing the number of simulations [37]. Indeed, the discretization steps set for the
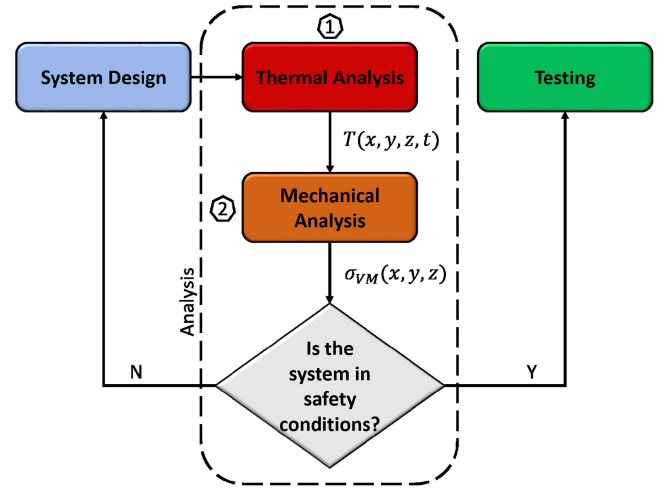

Fig. 5.   Skecth of the environmental and thermal conditions to which a typical satellite mission is exposed. During the orbit, the direct sun radiation (Q_{sun}), the albedo radiation (Q_a) and the infrared radiation from the earth (Q_{earth}) heat the spacecraft.

parameters limit the number of possible configurations which can be evaluated by the PSO. As a result, the algorithm will test the same position several times. Therefore, by saving the RL and fitness results in a matrix, each position will be simulated only once, and, if during the ith iteration a particle occupies again that position, the previous result is loaded and the simulation is not performed a second time. With reference to the scheme given in Fig. 2, this strategy strongly reduces the computational time, especially in the final iteration steps, where the particles are close to the minimum.

IV. MULTIPHYSICS ANALYSIS

Differently from the current state-of-the-art (Table I), we analyzed if and how the thermal conditions experienced during the LEO missions could affect the optimized CubeSat Ka-band antenna operations. Furthermore, the thermal analysis is oriented to understand if, given the chosen antenna geometry, it is possible that potentially risky mechanical stresses could lead to antenna damage or failure [11], [34], [44]. To these aims, the thermal analysis is coupled to the mechanical analysis, as shown in Fig. 5.

A. Thermal Analysis

Since the environment that the spacecraft encounters during its operational life largely varies during ground operation, the launch phase or when the orbit is reached [3], [45], as first, we will focus on the thermal analysis of the proposed antenna/array in LEO (Fig. 5). In Fig. 6 the thermal environment in LEO is summarized. During the orbit, three main heat sources may drastically affect the operation of the communication device; *i.e.* the direct sun radiation (Q_{sun}), the sunlight radiation reflected by the Earth, *i.e.,* the albedo (Q_a), and, finally, the infrared energy directly emitted from Earth's atmosphere or surface (Q_{earth}).
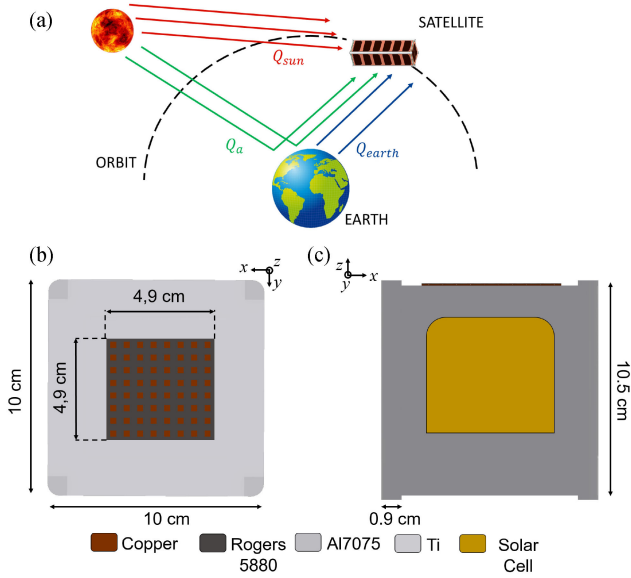
Fig. 6. a) Schematic description of the thermal conditions in a typical CubeSat mission. b) Top view of the CubeSat with the array mounted on the z^+-face. c) Lateral view of the 1 U CubeSat model with geometrical details.

For satellites operating at LEO distances of about 500–1000 km, the solar flux and the associated thermal load changes with the season of the year (*e.g.*, in summer $< Q_{sun} >= 1317 \pm 5$ Wm^{-2}, whilst in winter $< Q_{sun} >= 1414 \pm 5$ Wm^{-2}). The analytical expression for the solar radiation is [46]–[48]

$$Q_{sun} = \alpha G_s A_{sc} \cos \theta_s, \quad (8)$$

where α is the solar absorptance of the surface, A_{sc} is the surface area (~ 0.14 m^2) and θ_s is the angle formed by the solar rays and the surface normal.

The albedo flux is not constant during the orbits and varies depending on the surface properties of the Earth (*i.e.*, $Q_a = Q_a(t)$). It is a percentage of the radiation from the sun which is reflected into the deep space. The nominal albedo value is about $30\% \pm 10\%$ of the solar flux, for an average value of 237 ± 21 Wm^{-2}. In a more general form,

$$Q_a = aG_s A_{sc} F_{sc,p} \cos \phi \quad (9)$$

where a is the planetary albedo coefficient, G_s is the solar constant, ϕ the solar zenith angle ($-\pi/2 < \phi < \pi/2$), and $F_{sc,p}$ being the view factor between the CubeSat surface and the planet. The albedo coefficient and the view factors are evaluated according to the geometrical models found in [45], [46], [48]. The albedo coefficient strongly depends on the different missions analysed, since the orbit shape, height and inclination affect it [46]–[48].

Part of the solar flux to the Earth is re-emitted as longwave infra-red (IR) radiation, due to the finite Earth temperature, which can be considered as a black body having an effective temperature of about -22 °C (255 K), thus resulting in the following heat flux [45]

$$Q_{earth} = \epsilon A_s F_{sc,p} \sigma T_P^4, \quad (10)$$

where ϵ is the IR emissivity, σ is the Stefan-Boltzmann constant (5.67 Wm^{-2} K^{-4}), and T_P is the planetary black-body equivalent temperature.

The general thermal mathematical model for a satellite and its subsystems is a combination of heat transfer by conduction and radiation, with the environmental heating and cooling as boundary conditions [20]–[22]. For the physical situation of Fig. 6(b) and Fig. 6(c), the governing equation for the system temperature $T = T(x, y, z, t)$ is [20]–[22], [45]–[47]

$$\rho C_p \frac{\partial T}{\partial t} = -\nabla \cdot (k\nabla T) + \nabla \cdot [Q_{sun} + Q_{earth} + Q_a]$$
$$+ Q_{diss}, \quad (11)$$

where ρ is the material density (in kg $\cdot$ m^{-3}), C_p is the specific heat capacity (in Jkg $\cdot$ K^{-1}), t is the time (in s), k is the thermal conductivity (in Wm^{-1} K^{-1}) and Q_{diss} is the power dissipated by CubeSat electronic equipment (~ 3 Wm^{-3} [46]).

As a matter of fact, (11) is a non-linear second order partial differential equation. The non-linearity is due to the time-varying nature of the thermal loads and to the fact that the thermal parameters of the materials can be temperature-dependent. It is known that the thermal properties of materials such as copper [49]–[51] vary with temperature.

The radiation falling on and scattered from the outer surfaces was assumed to be diffuse [21]. The thermal radiation within the antenna cavities and the related absorption factors are accounted for in the thermal balance [45]. A Dirichlet boundary condition ($T = T_0$) is assumed at the initial time and the system was studied in two different initial states. We assumed the CubeSat and the communication system to be at a starting temperature of 20 °C (293 K) and -100 °C (173 K) at the initial time $t_0 = 0$. The system boundaries are not subject to heat transfer by air convection, so that the normal heat flux nulls, and the system is allowed to radiate heat into the surroundings [45]. The external temperature is assumed equal to -269 °C (4 K).

We consider as a case study a sun-synchronous circular orbit, with a right ascension of ascending node of about 106°, assuming an orbital height of 300 km and an inclination of $\sim 90°$ [46], [47]. In this configuration, the worst hot case is the sun pointing in the y_+ direction. The worst cold case occurs when the satellite is shadowed and the nadir is y_-. We simulated a total period of three orbits, with a 1 min time step. This transient analysis is sufficient for sizing the essential features of the heat transfer phenomena of the CubeSat subsystems [20], [21], [45]–[48]. The antennas are placed on the z_+ panel outside the satellite, as shown in Fig. 6(b) and Fig. 6(c). In this framework, the total power, in W, impinging on the CubeSat and communication system surfaces are shown in Fig. 7.

The heat transfer problem was solved by using the *Heat Transfer in Solids* package from the finite element method commercial software Comsol Multiphysics v5.5 (Comsol Inc., Burlinghton, MA, USA).

B. Mechanical Analysis of Thermal Stresses

The physical dimension changes due to thermal load and simulations with an applied coefficient of thermal expansion
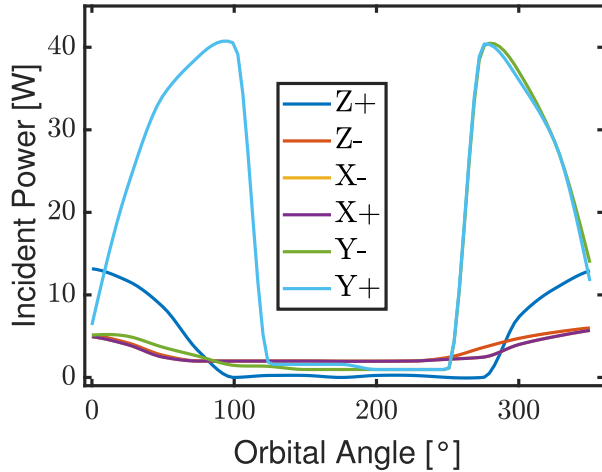
Fig. 7.   Impinging radiation, in W, on the six CubeSat faces for the case-study low earth orbit mission.

TABLE III
THERMAL PROPERTIES

Mat.	ρ (kg·m^{-3})	C_p (Jkg·K^{-1})	k (Wm^{-1}K^{-1})	α	ϵ
Al7075	2810	690	173	0.3	0.1
Solar Cell	2140	322	64	0.65	0.80
Ti	4500	540	2.2	0.6	0.9
RT/duroid 5880	2200	960	0.2	0.84	0.9
Copper	8940	385	400	0.5	0.5

must be performed to make sure the antenna will perform adequately [11], [15], [52], [53]. Indeed, for CubeSat application, the cosmic high-energy radiation can damage the mechanical properties of the polymeric substrate, thus increasing its brittleness, reducing the tensile strength, modulus and elongation [11]. Furthermore, under the thermal environment shown in Fig. 6, the spacecraft and its subsystems can undergo relevant deformations and mechanical stresses can be induced by the thermal gradients in the structure [20], [21], [45], [47]. Therefore, as shown in Fig. 5, we performed the mechanical analysis for the proposed optimized antenna design.

The mechanical analysis, following a damage-tolerant approach [54], [55], is performed by assuming that the linear thermoelasticity holds, so that relying on the infinitesimal strain-displacement relationship, for the continuity equation, the following constitutive equation for isotropic linear elastic material is solved [56], [57]

$$\underline{\sigma} = \underline{\underline{D}}\,\underline{\epsilon} \qquad (12)$$

where $\underline{\epsilon}$ and $\underline{\sigma}$ are the strains (ϵ_i, for $i = x, y$ and z, and $\gamma_{xy}, \gamma_{yz}, \gamma_{zx}$), and stresses ($\sigma_i$ and $\tau_{xy}, \tau_{yz}, \tau_{zx}$), respectively. The term $\underline{\underline{D}}$ is the stifness matrix [56]. For a given temperature gradient, the thermal strain vector of material can be written as [58]

$$\underline{\epsilon} = \frac{1 + \nu}{E}\underline{\sigma} - \frac{\nu}{E}\underline{\sigma} + \alpha_{CTE}\nabla T \qquad (13)$$

where ν is the Poisson's ratio, E is the Young's modulus (in Pa) and α_{CTE} denotes the thermal expansion coefficient (CTE), whilst ∇T is the temperature gradient vector, evaluated as change from the initial time step, where the initial stress and strain are set to zero [59]. A value of 0.4 for the Poisson ratio was assumed for the substrate [60] and its Young's modulus was assumed equal to 1 GPa [61]. For the copper a CTE of 16.7 ppm/°C was used [62], whilst the elastic modulus was set to 16 GPa and the Poisson ratio was assumed equal to 0.34 [61].

To solve (12), we assumed that the surface of the copper ground is constrained to the CubeSat and that the displacement nulls. At the interface between different materials the relative motion is assumed to be null [57].

We did not implement a multiphysics optimization procedure, in which the antenna constraints (*e.g.,* bandwidth, gain, size) are coupled to the thermal and mechanical aspects [63]–[66]. We assumed that mechanical coupling between strain and temperature in the heat conduction equation can be neglected by assuming a one-way resolution scheme [57]. In this framework, the shear rate values are not elevated, and that stationarity can be assumed. Since a mismatch between CTE coefficients of copper and Rogers substrate exists (Table III), the stresses would concentrate in this portion of the antenna (Fig. 1). This physical condition can be understood if framed into the bi-metallic theory [67]. The heat flux through plates, which are constrained at the interface, produces a state of strain that actually becomes a state of stress due to the boundary condition itself. Indeed, a change in the length of the patch sides due to an in-plane strain could occur during the LEO mission. The von Mises stress (σ_{VM}), defined as the second invariant of the stress tensor, is considered as a figure of merit for evaluating if the antenna system could suffer from any mechanical failure due to the induced thermal deformation [57].

The thermal stress analysis was performed in Comsol by using the *Structural Mechanics* module, in which the temperature field (T), computed from the heat transfer problem (Fig. 5), has been adopted.

V. RESULTS

This work deals with the design and analysis of a CubeSat stacked patch antenna working in suitable down- and uplink Ka-bands. A PSO algorithm to optimize the antenna geometry and match the stringent communication requirements for satellite applications has been proposed (Fig. 2). We analysed the convergence rate and the computational performance of our algorithm, then reported and studied the response of the optimized design.

A. Convergence

In Fig. 8 the convergence of the swarm to the optimized solution, in terms of fitness convergence to the global best, is reported. It can be noticed that after few iterations, the fitness value for the best swarm fitness and global best suddenly decreases. Fig. 9 shows the convergence of each antenna parameter during the optimization. In a way similar to Fig. 8, all the ten particles reach the optimal position after 501 iterations. The best solution
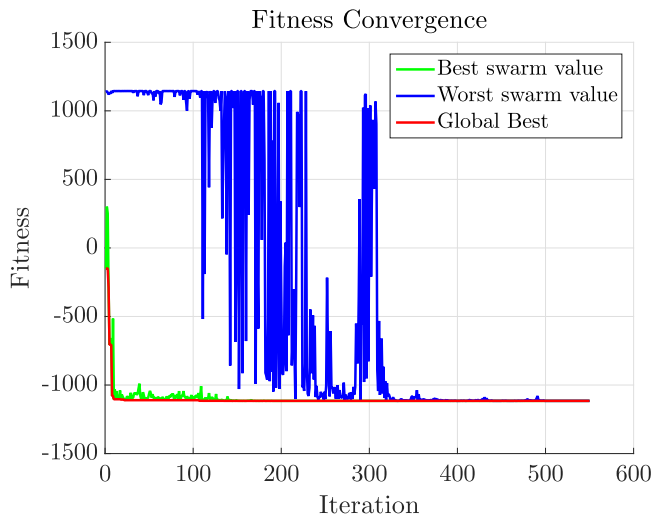
Fig. 8. Convergence of the swarm to the optimal solution. The best and worst fitness values assumed by the particles at each iteration are shown.
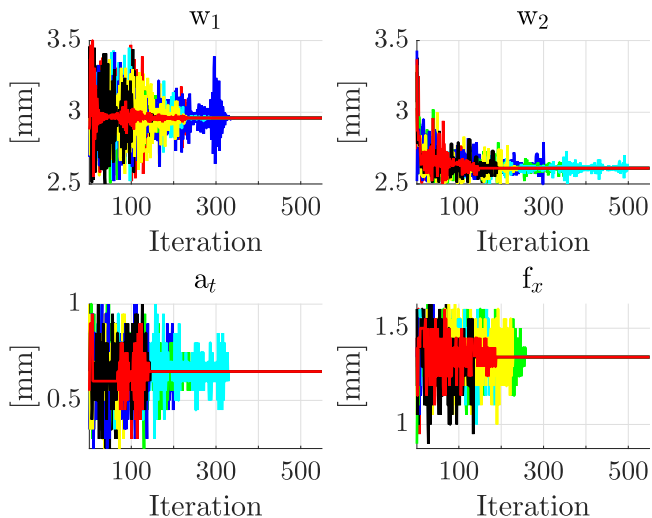

Fig. 9. Convergence of the antenna parameters: w_1, w_2, a_t and f_x.

TABLE IV
OPTIMAL SOLUTION: GEOMETRIC PARAMETERS AND PERFORMANCES

Param.	Value		Param.	[GHz]
w_1 [mm]	2.96		f_{min}	30.42
w_2 [mm]	2.61		f_{max}	35.95
a_t [mm]	0.65		BW	5.53
f_x [mm]	1.35			

of the geometrical parameters of the optimized antenna is listed in Table IV.

As regards the computational load, the overall optimization time depends on the number of configurations that the algorithm would encounter more than one time across the iterations. In Fig. 10, to better clarify this aspect, we reported the new (in blue) and the already tested (in yellow) configurations for each particle. In this way, it is possible to quantify the saved time with respect to an algorithm which simulates again the already
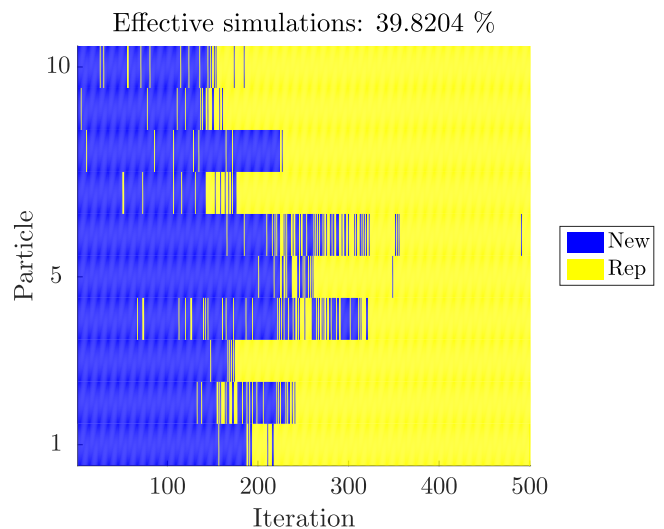

Fig. 10. Evaluation of how many algorithm iterations encounter new solution space positions (in blue, New), or position which have been already tested and do not need another full-wave analysis (in yellow, Rep).
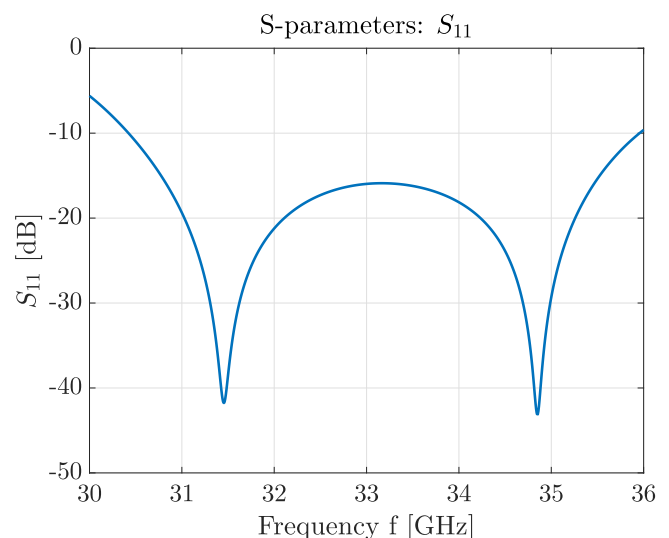

Fig. 11. S_{11} of the optimized antenna from 31 GHz to 35 GHz.

encountered positions. From Fig. 10, it results that only the 39.82% of the positions occupied by the swarm during the optimization is novel and needs to be effectively tested. Therefore, since the full-wave analysis is more time-consuming than the actual population movement, the use of saved results and of the matrix, shown in Fig. 10, allows to save more than 60% of the computational time.

B. Antenna and Array Performances

The parameters of the optimized geometry, for $\psi = 0.5$, and the resulting performance in terms of available BW are shown in Table IV. The resulting S_{11} is instead presented in Fig. 11. It is worth noting that the parameter $\psi = 0.5$ in the weighting function S_{11}^{wgt} drives to an optimized result with a margin of 5.8 dB in correspondence of the centre of the operating frequency
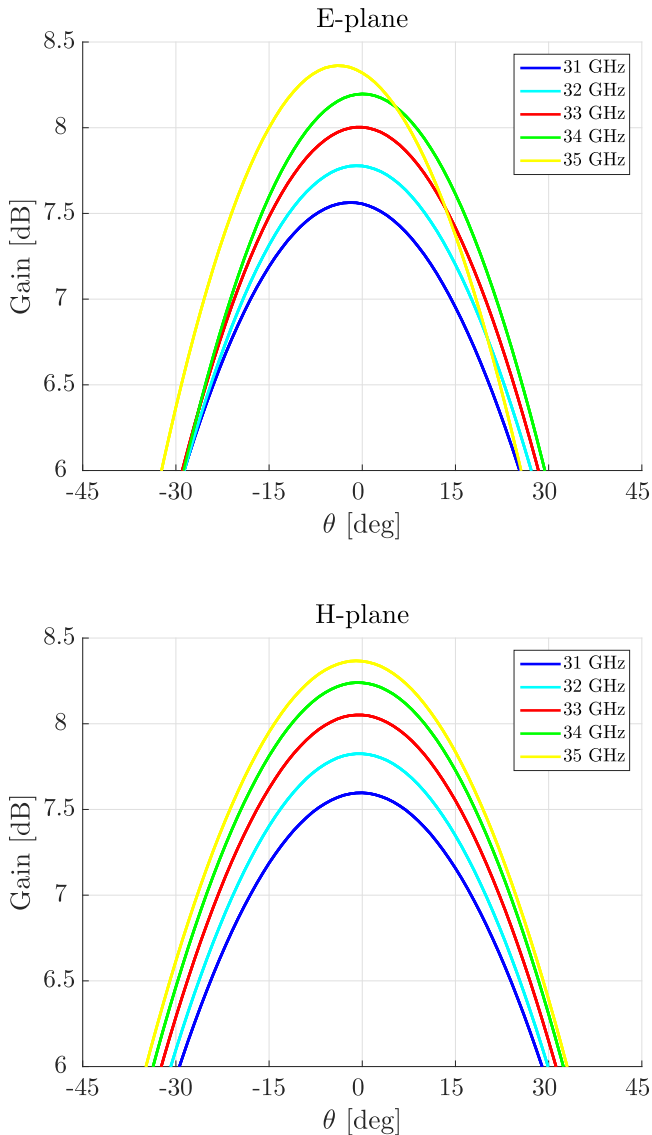
Fig. 13.   Broadside Gain over frequencies for different array size.

Fig. 12.   Gain of the optimized antenna over frequency (31-35 GHz). The main lobe keeps its direction over the operative frequency band.

Our planar antenna is proposed as an alternative to other bulky, complex CubeSat communication systems for the Ka-band available in the open literature (Table I). However, despite the optimized design presents an effective wideband operation, with a stable gain, high-gain antennas are mostly employed in CubeSat applications [6], [11]. Antennas array can be used to reach a gain of more than 20 dBi [10]. Therefore, in the following we analyse the possibility of using the optimized stacked antenna in an array and investigate its performance.

In Fig. 13, the broadside gain, provided at different frequencies in Ka-band, for different array sizes is provided. The distance between the elements was assumed equal to 6 mm. From Fig. 13, to obtain a high-gain, while maintaining a small size (5 cm in side), an array of 8x8 elements is sufficient to reach ∼26 dBi. The 8x8 array exhibits an antenna gain that is 2 dB higher than the antennas and solutions from [10], and comparable to the metasurface-based antenna from [14].

C. Multiphysics Analysis: Performance Over Temperature

The application of the antenna in CubeSat missions requires further investigation of its performance during the LEO operation. To this aim, the optimized 8x8 antenna array thermal and mechanical behaviour was simulated over 3 orbits. The average array temperature is reported in Fig. 14(a). It can be noticed that, under the cyclic thermal load perturbation shown in Fig. 7, despite the different initial temperature conditions, the temperature response of the spacecraft model results in a limit cycle [20], which approaches a maximum value of ∼ 50 °C and a lower bound of about 10 °C. However, the curves from Fig. 14(a) are the average over the 64 antenna elements, as shown in Fig. 14(b)-(d). The inner copper patch (Patch 1, in Fig. 1) experiences a higher temperature than the external patch (Patch 2, in Fig. 1). Indeed, the latter tends to equilibrate with the surroundings at 4 K. In the cyclic limit, as shown in Fig. 14(d), the maximum temperatures experienced by the optimized array

band. The BW is about 16.6%, which is much larger than the requirement of 1.6% for the Ka-band downlink [14]. This result, compared to the state-of-the-art solutions reported in Table I, is outstanding and outperforms the patch array from [10], but also the reflectors reported in [6], [7].

As regards the far-field pattern, the antenna should maintain the main lobe direction in the whole operative frequency bands. To evaluate if such a condition is verified, in Fig. 12 the far-field patterns, for both E- and H-planes, are reported at different frequencies (31-35 GHz). From Fig. 12, the antenna maintains its pointing direction over the Ka-bands, apart for a little displacement lower than 5° at the upper frequency along the E-plane. As discussed by Buttazzoni *et al.* [10], the far-field stability over frequency can avoid issues related to the satellites operation, which could lead to illuminate different areas at different frequencies with the same antenna.
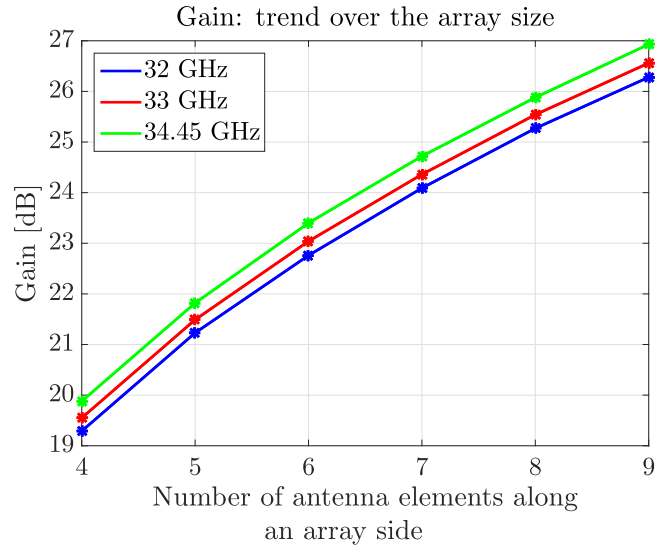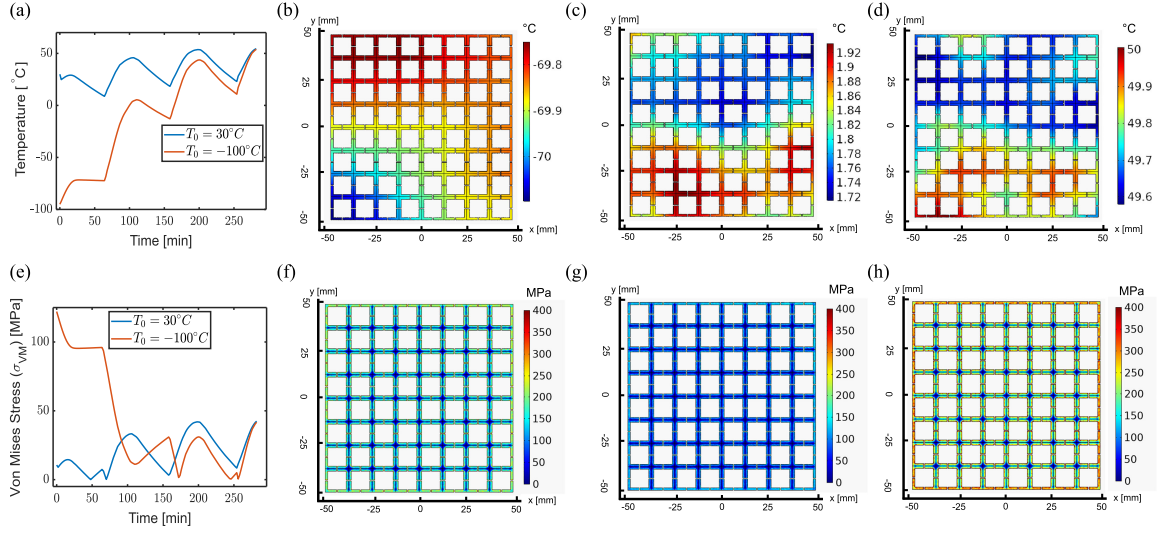
Fig. 14. a) Average array temperature for the different initial temperatures (T_0) of 30 °C and -100 °C, during the orbital period. b) 2D temperature distribution on the xy-plane of the array ($z = a_t + 350\mu$m) at $t = 60$ min, for $T_0 = -100$°C. c) 2D temperature distribution on the xy-plane of the array ($z = a_t + 350\mu$m) at $t = 60$ min, for $T_0 = 30$°C. d) 2D temperature distribution on the xy-plane of the array ($z = a_t + 350\mu$m) at $t = 280$ min. e) Average von Mises stresses for the different initial temperatures (T_0) of 30 °C and -100 °C, during the orbital period. f) 2D pattern of the von Mises stresses on the xy-plane of the array ($z = a_t + 350\mu$m) at $t = 60$ min, for $T_0 = -100$°C. g) 2D pattern of the von Mises stresses on the xy-plane of the array ($z = a_t + 350\mu$m) at $t = 60$ min, for $T_0 = 30$°C. h) 2D pattern of the von Mises stresses on the xy-plane of the array ($z = a_t + 350\mu$m) at $t = 280$ min.

are well below the threshold of about 200 °C, which is typical of commercial Prepreg resins (*e.g.,* SpeedWave ^{TM} 300P), that could be used for manufacture the stacked antennas [68]. The spatio-temporal temperature patterns observed qualitatively agree with the numerical simulations reported by [45], [69]. Furthermore, given the small size ($\sim$5 cm $\times$ 5 cm) of the antenna, the thermal gradients in the system are relatively small (*e.g.,* maximum 0.4 °C $\cdot$ cm^{-1}) [20], [21], [45], [69].

In this framework, the performances of a single antenna element have been tested by varying the material properties over the temperature, to get the distribution of the antenna response over the heat transfer condition reported in Fig. 14. In detail, we assumed a linear variation of the permittivity pattern over temperature [25], whereas the copper conductivity over temperature was taken from [49], [50]. Fig. 15 displays the impact of the temperature variation on the Return Loss. The higher the temperature, the higher, and shifted up in frequency, the Return Loss values. By observing Fig. 15, even though the temperature modifies the antennas behaviour, with a frequency shift of 340 MHz in the operative -10 dB frequency band, the optimized wide bandwidth guarantees that the antenna operation still covers the downlink (31.8–32.3 GHz) and uplink (34.2–34.7 GHz) frequency bands of the deep-space Ka band, with a value of the RL higher than 15 dB.

By refining the analysis, in Fig. 16 it is shown the far field pattern of the antenna in the two deep-space Ka bands, at 32 and 34.45 GHz. The gain is poorly affected ($<$1 dB) by the temperature excursion, as demonstrated by the overlapping curves shown in Fig. 16. This result provides a high level of confidence on the antenna performance as the temperature changes.

These results confirm that an optimization process oriented to the frequency band maximization (with in the same time the constraint on the central frequency RL value) allows obtaining an
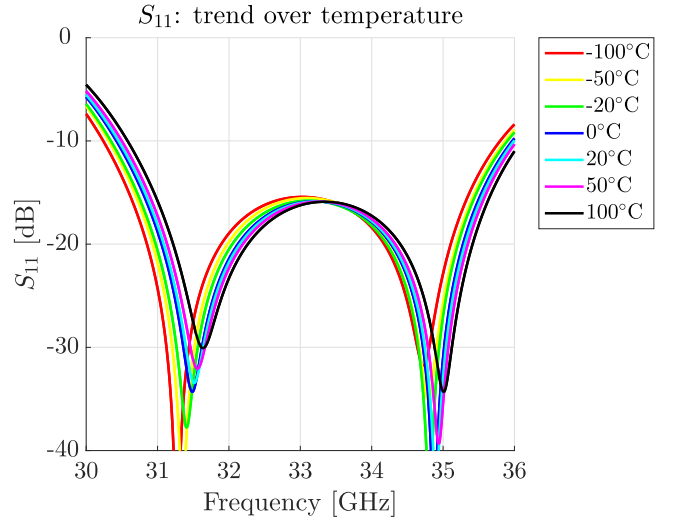
Fig. 15. S_{11} of the antenna element at different temperatures. It can be noticed that the temperature raise results in a shift towards higher frequencies.

antenna with a good tolerance with respect to the environmental conditions, as well as better manufacturingxbrk tolerance.

D. Temperature Evolution and Thermal Stress During LEO Operations

The induced average thermal stresses on the 8x8 array, for the two different initial conditions, are shown in Fig. 14(e), and the bidimensional patterns are reported in Fig. 14(f)-(h). The σ_{VM} figure of merit accounts for the distortional energy caused by a stress state, equivalent to an actual combined state of stress [67], which is, in our case, the tensional state induced

Fig. 16. Broadside Gain over temperature in the two deep-space Ka frequency bands.
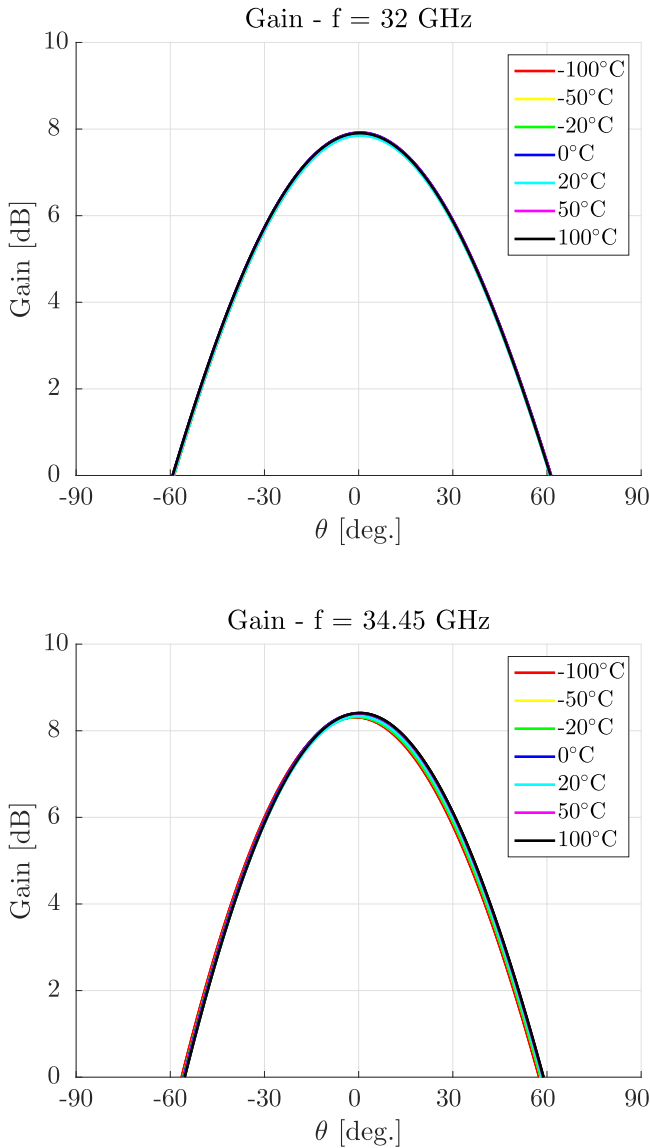
by the temperature gradients, shown in Fig. 14(b)-(d), induced in the array exposed to the different thermal loads (Fig. 7). In this framework, the von Mises stresses on the array elements are in the range of 47–120 MPa (Fig. 14(e)), for the hot and cold case studies. After about 200 min the proposed stacked patch antenna array equilibrates with the surroundings and reaches the quasi-steady state under the cyclic loading. In this condition, the level of average stresses is below 50 MPa. The σ_{VM} values can be critical for the substrate material maximum acceptable stresses, which, for the Rogers RT/duroid 5880, are on the order of 23-237 MPa [25]. However, the cold case, for $T_0 = -100°C$, presents the largest temperature gradients in the array (Fig. 14(b)), and therefore the largest average σ_{VM} values are obtained, as shown in Fig. 14(f). The stresses are concentrated at the corners of the metal ring (according to classical structural mechanic theory [67]), and at the outer boundaries of the array,

then relaxing and lowering moving towards the center. The average stress values observed in Fig. 14(f)–(h) could represent a risk of failure due to the detachment between the metal ring and the upper patch substrate. Indeed, commercial prepreg and epoxy resins could be used for the antenna assembly (Fig. 1). For instance, the SpeedWave ^{TM} 300P Prepreg resin can tolerate a maximum of 20–35 MPa [70]. In the thermal and mechanical conditions at regime (after 280 min), shown in Figs. 14(d) and 14(h), another technological solution for the manufacturing would be of interest. With our thermo-mechanical analysis and the findings reported in Fig. 14, we can infer that the use of other epoxy resins capable of reaching high tensile, shear and flexural stresses, in the range 65-450 Mpa, such as the on-the-shelf SX10EVO [71]–[73], would ensure robustness and reliability to the proposed solution in the early mission stages. On the other hand, it must be highlighted that the stresses and strains in the 8x8 antenna array, in the cyclic limit regime, can be easily managed with the use of mechanically performing resins [71]–[73] or by adopting current adaptive temperature control strategies [21], [45]. The stress patterns, shown Fig. 14(e)-(h), result in a negligible bending (ϵ_z) of the antenna array of about 0.1-0.25 μm [67], which would not affect the radiating performances of the antenna during the LEO mission.

VI. CONCLUSION

CubeSats are low-cost nano-satellites increasingly used for remote sensing, telecommunications, deep-space communication and interplanetary missions in LEO. Nowadays, for CubeSat applications the Ka-band (31-35 GHz for down- and uplink frequencies) is investigated. The technology is at an early stage, thus new engineering solutions are necessary. In particular, this work dealt with the optimized design of a stacked patch antenna for CubeSat applications. The antenna materials and topology were selected to satisfy the compliance with mechanical and thermal spacecraft requirements. In this framework, a PSO algorithm for bandwidth optimization was proposed and an optimized stacked antenna able to work in both downlink and uplink Ka-bands was obtained. The results show that the proper setting of the objective function parameters allows shaping the optimized performance according to the design requirements. A wideband operation is achieved, larger than 5 GHz, with a broadside radiation and an almost constant gain. The proposed solution, if deployed in a 1 U CubeSat in a 8x8 array configuration, can result in a lightweight, small-sized (∼5x5 cm), high-gain (26 dB) communication system, which can compete with the state-of-the-art solutions.

To provide a quantitative measure of the feasibility of optimized antenna arrays for CubeSat applications, we performed the one-way coupled thermal and mechanical analysis during a typical LEO mission. We found that the array, under different thermal conditions and loads, does not reach the potentially risky temperatures for its materials. The temperature-induced stresses, on the other hand, can present a failure possibility, due to large contractions in extremely cold orbital phases, thus probably calling for the use of current temperature control systems.

The optimization algorithm proposed in this work can be of interest for the design of other antenna at different frequencies, such as those to be used for fifth- and sixth-generation technology applications. For instance, given that the future of CubeSat antenna designs is already driven by emerging applications, such as 5G hybrid satellite-terrestrial (5 G S-T) architectures, the proposed solution could be used to study how to expand the current CubeSat capabilities, by introducing multibeam and beam steering functionalities.

ACKNOWLEDGMENT

REFERENCES

[1] G. Capovilla, E. Cestino, L. M. Reyneri, and G. Romeo, "Modular multifunctional composite structure for CubeSat applications: Preliminary design and structural analysis," *Aerospace*, vol. 7, no. 2, 2020, Art. no. 17. [Online]. Avilable: https://www.mdpi.com/2226-4310/7/2/17

[2] N. Saeed, A. Elzanaty, H. Almorad, H. Dahrouj, T. Y. Al-Naffouri, and M.-S. Alouini, "CubeSat communications: Recent advances and future challenges," *IEEE Commun. Surv Tut.*, vol. 22, no. 3, pp. 1839–1862, Jul.–Sep. 2020.

[3] G. Broccia, "CubeSats in low Earth orbit: Perils and countermeasures," 2021, *arXiv:2105.00107*.

[4] C. Cappelletti and D. Robson, "CubeSat missions and applications," in *CubeSat Handbook*. Amsterdam, The Netherlands: Elsevier, 2021, pp. 53–65.

[5] N. Chahat, J. Sauder, M. Mitchell, N. Beidleman, and G. Freebury, "One-meter deployable mesh reflector for deep-space network telecommunication at X-band and Ka-band," *IEEE Trans. Antennas Propag.*, vol. 68, no. 2, pp. 727–735, Feb. 2020.

[6] S. Abulgasem, F. Tubbal, R. Raad, P. I. Theoharis, S. Lu, and S. Iranmanesh, "Antenna designs for CubeSats: A review," *IEEE Access*, vol. 9, pp. 45 289–45324, 2021.

[7] N. Chahat, R. E. Hodges, J. Sauder, M. Thomson, E. Peral, and Y. Rahmat-Samii, "CubeSat deployable Ka-band mesh reflector antenna development for Earth science missions," *IEEE Trans. Antennas Propag.*, vol. 64, no. 6, pp. 2083–2093, Jun. 2016.

[8] N. Chahat, J. Sauder, M. Mitchell, N. Beidleman, and G. Freebury, "One-meter deployable mesh reflector for deep space network telecommunication at X-and Ka-band," in *Proc. 13th Eur. Conf. Antennas Propag.*, 2019, pp. 1–4.

[9] NASA, "State of the art: Small spacecraft technology."

[10] G. Buttazzoni, M. Comisso, A. Cuttin, M. Fragiacomo, R. Vescovo, and R. V. Gatti, "Reconfigurable phased antenna array for extending CubeSat operations to Ka-band: Design and feasibility," *Acta Astronautica*, vol. 137, pp. 114–121, 2017.

[11] N. Chahat, *CubeSat Antenna Design*. Hoboken, NJ, USA: Wiley, pp. 233–253, 2021.

[12] N. Chahat, R. E. Hodges, J. Sauder, M. Thomson, and Y. Rahmat-Samii, "The deep-space network telecommunication CubeSat antenna: Using the deployable Ka-band mesh reflector antenna," *IEEE Antennas Propag. Mag.*, vol. 59, no. 2, pp. 31–38, Apr. 2017.

[13] R. E. Hodges, D. J. Hoppe, M. J. Radway, and N. E. Chahat, "Novel deployable reflectarray antennas for CubeSat communications," in *Proc. IEEE MTT-S Int. Microw. Symp.*, 2015, pp. 1–4.

[14] D. Gonzalez-Ovejero, N. Chahat, R. Sauleau, G. Chattopadhyay, S. Maci, and M. Ettorre, "Additive manufactured metal-only modulated metasurface antennas," *IEEE Trans. Antennas Propag.*, vol. 66, no. 11, pp. 6106–6114, Nov. 2018.

[15] R. M. Rodríguez-Osorio and E. F. Ramírez, "A hands-on education project: Antenna design for inter-CubeSat communications," *IEEE Antennas Propag. Mag.*, vol. 54, no. 5, pp. 211–224, Oct. 2012.

[16] S. C. Pavone, M. Casaletti, and M. Albani, "Automatic design of a CP fan-beam linear slotted array in SIW technology," *IEEE Access*, vol. 7, pp. 155977–155985, 2019.

[17] J. King, J. Ness, G. Bonin, M. Brett, and D. Faber, "c," 2012. [Online]. Available: https://digitalcommons.usu.edu/smallsat/2012/all2012/54/

[18] R. E. Hodges, M. J. Radway, A. Toorian, D. J. Hoppe, B. Shah, and A. E. Kalman, "ISARA-Integrated solar array and reflectarray CubeSat deployable Ka-band antenna," in *Proc. IEEE Int. Symp. Antennas Propag. USNC/URSI Nat. Radio Sci. Meeting*, 2015, pp. 2141–2142.

[19] R. Głogowski, J.-F. Zürcher, J. R. Mosig, and C. Peixeiro, "Circularly polarized aperture coupled stacked patch antenna element for Ka-band," in *Proc. IEEE Int. Symp. Antennas Propag.*, 2011, pp. 911–914.

[20] J.-R. Tsai, "Overview of satellite thermal analytical model," *J. Spacecraft Rockets*, vol. 41, no. 1, pp. 120–125, 2004.

[21] N. Anh, N. Hieu, P. Chung, and N. Anh, "Thermal radiation analysis for small satellites with single-node model using techniques of equivalent linearization," *Appl. Thermal Eng.*, vol. 94, pp. 607–614, 2016.

[22] H. Sundu and N. Döner, "Detailed thermal design and control of an observation satellite in low Earth orbit," *Eur. Mech. Sci.*, vol. 4, no. 4, pp. 171–178, 2020.

[23] Esatan, "Thermal desktop," [Online]. Available: https://www.crtech.com/products/thermal-desktop

[24] Systema, "Systema thermica," [Online]. Available: https://www.systema.airbusdefenceandspace.com/products/thermica.html

[25] M. Simone, A. Fanti, G. Valente, G. Montisci, R. Ghiani, and G. Mazzarella, "A compact in-line waveguide-to-microstrip transition in the Q-band for radio astronomy applications," *Electronics*, vol. 7, no. 2, 2018, Art. no. 24. [Online]. Avilable: https://www.mdpi.com/2079-9292/7/2/24

[26] B.-L. Ooi, S. Qin, and M.-S. Leong, "Novel design of broad-band stacked patch antenna," *IEEE Trans. Antennas Propag.*, vol. 50, no. 10, pp. 1391–1395, Oct. 2002.

[27] M. Matin, B. Sharif, and C. Tsimenidis, "Probe fed stacked patch antenna for wideband applications," *IEEE Trans. Antennas Propag.*, vol. 55, no. 8, pp. 2385–2388, Aug. 2007.

[28] M. Ali, A. T. Sayem, and V. K. Kunda, "A reconfigurable stacked microstrip patch antenna for satellite and terrestrial links," *IEEE Trans. Veh. Technol.*, vol. 56, no. 2, pp. 426–435, Mar. 2007.

[29] H. Yang, Y. Fan, and X. Liu, "A compact dual-band stacked patch antenna with dual circular polarizations for BeiDou navigation satellite systems," *IEEE Antennas Wireless Propag. Lett.*, vol. 18, no. 7, pp. 1472–1476, Jul. 2019.

[30] M. Khalily, R. Tafazolli, P. Xiao, and A. A. Kishk, "Broadband mm-Wave microstrip array antenna with improved radiation characteristics for different 5G applications," *IEEE Trans. Antennas Propag.*, vol. 66, no. 9, pp. 4641–4647, Sep. 2018.

[31] T. Chaloun, V. Ziegler, and W. Menzel, "Design of a dual-polarized stacked patch antenna for wide-angle scanning reflect arrays," *IEEE Trans. Antennas Propag.*, vol. 64, no. 8, pp. 3380–3390, Aug. 2016.

[32] N. Chahat *et al.*, "Advanced CubeSat antennas for deep space and Earth science missions," *IEEE Antennas Propag. Mag.*, vol. 61, no. 5, pp. 37–46, Oct. 2019.

[33] J. A. V. Vilán, F. A. Agelet, M. L. Estévez, and A. G. Muiño, "Flight results: Reliability and lifetime of the polymeric 3D-printed antenna deployment mechanism installed on Xatcobeo & Humsat-D," *Acta Astronautica*, vol. 107, pp. 290–300, 2015.

[34] G. Roethlisberger, F. Jordan, A. Servonet, M. Borgeaud, R. Krpoun, and H. Shea, "Advanced methods for structural machining and solar cell bonding allowing high system integration and their demonstration on a Pico-satellite," 2008.

[35] B. D. Dunn, "Spacecraft manufacturing-failure prevention and the application of material analysis and metallography," in *Materials and Processes*. Berlin, Germany: Springer, 2016, pp. 115–245.

[36] M. Kovaleva, D. Bulger, and K. P. Esselle, "Comparative study of optimization algorithms on the design of broadband antennas," *IEEE J. Multiscale Multiphys. Comput. Tech.*, vol. 5, pp. 89–98, Oct. 2020.

[37] Y. G. Rabobason *et al.*, "Design of flexible passive antenna array on Kapton substrate," *Prog. Electromagn. Res. C*, vol. 63, pp. 105–117, 2016.

[38] D. J. Kern, D. H. Werner, and M. Lisovich, "Metaferrites: Using electromagnetic bandgap structures to synthesize metamaterial ferrites," *IEEE Trans. Antennas Propag.*, vol. 53, no. 4, pp. 1382–1389, Apr. 2005.

[39] J. Robinson and Y. Rahmat-Samii, "Particle swarm optimization in electromagnetics," *IEEE Trans. Antennas Propag.*, vol. 52, no. 2, pp. 397–407, Feb. 2004.

[40] Y. Shi *et al.*, "Particle swarm optimization: Developments, applications and resources," in *Proc. Congr. Evol. Computation*, 2001, vol. 1, pp. 81–86.

[41] M. Simone, A. Fanti, M. B. Lodi, T. Pisanu, and G. Mazzarella, "An in-line coaxial-to-waveguide transition for Q-band single-feed-per-beam antenna systems," *Appl. Sci.*, vol. 11, no. 6, p. 2524, 2021.

[42] Z. Xu, B. Ravelo, and O. Maurice, "Multiphysics tensorial network analysis applied to PCB interconnect fatigue under thermal cycle aggression," *IEEE Trans. Electromagn. Compat.*, vol. 61, no. 4, pp. 1253–1260, Aug. 2019.

[43] S. Corpino, M. Caldera, F. Nichele, M. Masoero, and N. Viola, "Thermal design and analysis of a nanosatellite in low Earth orbit," *Acta Astronautica*, vol. 115, pp. 247–261, 2015.

[44] M. M. Garzon, "Development and analysis of the thermal design for the OSIRIS-3U CubeSat," 2012.

[45] G. Marraffa, "Thermal analysis of 6U CubeSats," Ph.D. dissertation, Politecnico di Torino, 2019.

[46] G. Broccia, "Solar radiation profiles for a 3U CubeSat in LEO," 2021, *arXiv:2105.09734*.

[47] R. Berman and D. K. C. Macdonald, "The thermal and electrical conductivity of copper at low temperatures," *Proc. Roy. Soc. London. Ser. A. Math. Phys. Sci.*, vol. 211, no. 1104, pp. 122–128, 1952.

[48] G. White, "The thermal and electrical conductivity of copper at low temperatures," *Australian J. Phys.*, vol. 6, no. 4, pp. 397–404, 1953.

[49] F. Cardarelli, *Materials Handbook*. Berlin, Germany: Springer, pp. 273–284, 2018.

[50] M. Sakovsky, I. Maqueda Jimenez, C. Karl, S. Pellegrino, and J. Costantine, "Dual-matrix composite wideband antenna structures for cubesats," in *Proc. 2nd AIAA Spacecraft Struct. Conf.*, 2015, Art. no. 0944. [Online]. Avilable: https://arc.aiaa.org/doi/abs/10.2514/6.2015-0944

[51] T. Yekan and R. Baktur, "Conformal integrated solar panel antennas: Two effective integration methods of antennas with solar cells," *IEEE Antennas Propag. Mag.*, vol. 59, no. 2, pp. 69–78, Apr. 2017.

[52] A. Ampatzoglou and V. Kostopoulos, "Design, analysis, optimization, manufacturing, and testing of a 2U CubeSat," *Int. J. Aerosp. Eng.*, vol. 2018, 2018. [Online]. Avilable: https://www.hindawi.com/journals/ijae/2018/9724263/

[53] P. Fernandes, R. Pinto, and N. Correia, "Design and optimization of self-deployable damage tolerant composite structures: A review," *Composites Part B: Eng.*, 2021, Art. no. 109029. [Online]. Avilable: https://www.sciencedirect.com/science/article/pii/S1359836821004133

[54] J. Zhang, M. O. Bloomfield, J.-Q. Lu, R. J. Gutmann, and T. S. Cale, "Modeling thermal stresses in 3-D IC interwafer interconnects," *IEEE Trans. Semicond. Manuf.*, vol. 19, no. 4, pp. 437–448, Nov. 2006.

[55] T. Lu and J.-M. Jin, "Coupled electrical-thermal-mechanical simulation for the reliability analysis of large-scale 3-D interconnects," *IEEE Trans. Compon. Packag. Manuf. Technol.*, vol. 7, no. 2, pp. 229–237, Feb. 2017.

[56] L.-K. Chiang, H.-C. Liu, Y.-H. Shiu, C.-H. Lee, and R.-Y. Lee, "Thermo-electrochemical and thermal stress analysis for an anode-supported SOFC cell," *Renewable Energy*, vol. 33, no. 12, pp. 2580–2588, 2008.

[57] P. Keangin, T. Wessapan, and P. Rattanadecho, "Analysis of heat transfer in deformed liver cancer modeling treated using a microwave coaxial antenna," *Appl. Thermal Eng.*, vol. 31, no. 16, pp. 3243–3254, 2011.

[58] K. Xu, L. Xie, S. Xue, K. Xue, and G. Wan, "Influence of transverse deformation on resonant frequency of patch antenna," in *Proc. IEEE Sensors Appl. Symp.*, 2018, pp. 1–6.

[59] A. K. Jha and P. D. Swami, "Technique of material design for patch antenna substrate using frequency dependent material setup," in *Proc. IEEE Int. Conf. Comput., Power Commun. Technol.*, 2020, pp. 820–823.

[60] C. Hagart-Alexander, "Chapter 21 - Temperature measurement," in *Instrumentation Reference Book*, 4th ed., W. Boyes, Ed. Boston, MA, USA: Butterworth-Heinemann, 2010, pp. 269–326. [Online]. Available: https://www.sciencedirect.com/science/article/pii/B9780750683081000218

[61] L. Song *et al.*, "Efficient computation of real-time distorted conformal load-bearing antenna structure under dynamic mechanical load based on modal superposition," *IEEE J. Multiscale Multiphys. Comput. Tech.*, vol. 3, pp. 246–254, 2018.

[62] G. P. Szakmany, A. O. Orlov, G. H. Bernstein, M. Lin, and W. Porod, "Multiphysics THz antenna simulations," *IEEE J. Multiscale Multiphys. Comput. Tech.*, vol. 3, pp. 289–294, 2018.

[63] B. Ravelo, N. Peyret, O. Penas, and T. Davin, "Multiphysics analysis of hemispherical bulk conductor hertzian contact under uniaxial mechanical load," *IEEE J. Multiscale Multiphys. Comput. Tech.*, vol. 4, pp. 171–179, 2019.

[64] B. Ravelo, "Multiphysics model of microstrip structure under high voltage pulse excitation," *IEEE J. Multiscale Multiphys. Comput. Tech.*, vol. 3, pp. 88–96, 2018.

[65] R. G. Budynas and A. M. Sadegh, *Roark's Formulas for Stress and Strain*. New York, NY, USA: McGraw-Hill, 2020.

[66] P. J. Klich and C. E. Cockrell, "Mechanical properties of a fiberglass prepreg system at cryogenic and other temperatures," *AIAA J.*, vol. 21, no. 12, pp. 1722–1728, 1983.

[67] M. Bulut, "Thermal design, analysis, and testing of the first Turkish 3U communication CubeSat in low Earth orbit," *J. Thermal Anal. Calorimetry*, vol. 143, no. 6, pp. 4341–4353, 2021.

[68] S. Sethi and B. C. Ray, "An assessment of mechanical behavior and fractography study of glass/epoxy composites at different temperatures and loading speeds," *Mater. Des.*, vol. 64, pp. 160–165, 2014.

[69] G. Pitarresi, D. Tumino, and A. Mancuso, "Thermo-mechanical behaviour of flax-fibre reinforced epoxy laminates for industrial applications," *Materials*, vol. 8, no. 11, pp. 7371–7388, 2015.

[70] L. Boccarusso, M. Durante, A. Langella, and F. M. C. Minutolo, "FE analysis of low density hemp/epoxy composites produced by a new continuous process," *Procedia CIRP*, vol. 67, pp. 428–433, 2018.

[71] V. Esperto, M. Durante, P. Carlone, and L. Carrino, "Resin microwave preheating in liquid composite molding process," *AIP Conf. Proc.*, vol. 2113, no. 1, 2019, Art. no. 110007. [Online]. Avilable: https://aip.scitation.org/doi/abs/10.1063/1.5112650

Marco Simone received the master's degree in electronic engineering and the Ph.D. degree in electronic and computer engineering from the University of Cagliari, Cagliari, Italy, in 2011 and 2016, respectively. He was a Visiting Ph.D. Student with the Queen Mary University of London, London, U.K., in 2015, and a Postdoctoral Research Assistant during 2016–2017 in the same University, with Antennas and Electromagnetics Research Group. Since 2017, he has been an Associate Researcher with the Laboratory of Applied Electromagnetics, University of Cagliari. His research interests include optimization techniques applied to electromagnetics problems, microwave components design for radioastronomy applications, and antennas design.

Matteo Bruno Lodi (Graduate Student Member, IEEE) received the bachelor's degree in biomedical engineering from the University of Cagliari, Cagliari, Italy, in 2016 and the master's degree in biomedical engineering from Politecnico di Torino, Turin, Italy, in 2018. He is currently working toward the Ph.D. degree in electronic engineering and computer science with the University of Cagliari. His research activity deals with the modeling of bioelectromagnetic phenomena, especially hyperthermia treatment, the study, manufacturing, and synthesis of magnetic biomaterials for tissue engineering applications, and the use of microwave for biotechnology and environmental applications. He was awarded as Young Scientists at General Assembly and Scientific Symposium of URSI 2020 and 2021. He has been appointed as the Representative for the Young Professionals of IEEE Region 8 Nanotechnology Council. He is a Member of the Editorial Board of the IEEE Future Directions Technology Policy and Ethics newsletter.

Santi Concetto Pavone (Senior Member, IEEE) received the B.Sc. and M.Sc. degrees (summa cum laude) in electronics engineering from the University of Messina, Messina, Italy, in 2010 and 2012, respectively, and the Ph.D. degree (with the additional label of "Doctor Europaeus") in information engineering and science (electromagnetics engineering) from the University of Siena, Siena, Italy, in 2015. He was a Visiting Ph.D. Student and an Assistant Professor with the Institut d'Électronique et de Télécommunications de Rennes, Université de Rennes 1, Rennes, France, in 2015 and 2020, respectively. From 2016 to July 2019, he was an Associate Researcher with the Laboratory of Applied Electromagnetics, University of Siena. Since August 2019, he has been an Assistant Professor with the Department of Electrical, Electronics, and Information Engineering, University of Catania, Italy. His current research interests include fundamental electromagnetic theory, scattering theory, RADAR design at millimeter waves, high-frequency techniques, focusing systems, nondiffractive localized pulses, and reconfigurable antennas. He was the recipient of the ESF Research Networking Programme NEWFOCUS Scholarship in 2015 and the IEEE Antennas and Propagation Society Student Award, Chapter Central-Southern Italy, in 2014. In 2017, he was a finalist for the Best Paper Award in Electromagnetics and Antenna Theory at the 11th European Conference on Antennas and Propagation, Paris. In 2018, he was the co-recipient of the Best Paper Award in Electromagnetics and Antenna Theory at the 12th European Conference on Antennas and Propagation, London, U.K. In 2019, he was the recipient of the Young Scientist Award at the 41st Progress in Electromagnetics Research Symposium, held in Rome, Italy. In 2020, he got the National Scientific Habilitation for Associate Professorship of Electromagnetic Fields by the Italian Ministry of University and Research, and he was selected among the outstanding 100 reviewers for the IEEE TRANSACTIONS ON ANTENNAS AND PROPAGATION from June 2019 to May 2020. In 2021, he was the recipient of the Young Scientist Award at the XXXIV General Assembly and Scientific Symposium of the International Union of Radio Science (URSI-GASS 2021). He is an Associate Editor for the IEEE ACCESS and *IET Electronics Letters*.

Nicola Curreli after the M.Sc. degree from the University of Genoa (Genoa, Italy), in 2016, received the Ph.D. degree in electronic engineering, from the University of Cagliari (Cagliari, Italy) and the Italian Institute of Technology - IIT (Genoa, Italy), in 2020. In 2019 he was a Visiting Researcher with the Physics and Mechanical Engineering Departments with Columbia University, New York, NY, USA. After the Ph.D., he held a fellow position at Graphene Labs–IIT in the WP12 (Energy storage) of the Graphene Core 2 project - Graphene flagship. His research activity includes the study of low-dimensional materials, their characterization and their application in the field of photonics, as well as the design, implementation, and analysis of linear and nonlinear integrated optical, microwave devices and antennas.

Giuseppe Mazzarella (Senior Member, IEEE) graduated with (summa with laude) in electronic engineering from the Universitá Federico II of Naples, Naples, Italy, in 1984 and the Ph.D. degree in electronic engineering and computer science in 1989. In 1990, he became an Assistant Professor with the Dipartimento di Ingegneria Elettronica, Universitá Federico II of Naples. Since 1992, he has been with the Dipartimento di Ingegneria Elettrica ed Elettronica, Universitá di Cagliari, first as an Associate Professor and then, since 2000, as Full Professor, teaching courses in Electromagnetics, Microwave, Antennas and Remote Sensing. He is the author or coauthor of more than 70 papers in international journals. His research interests mainly include efficient design of large arrays of slots, power synthesis of array factor, with emphasis on inclusion of constraints, microwave holography techniques for the diagnosis of large reflector antennas, use of evolutionary programming for the solution of inverse problems, in particular problems of synthesis of antennas and periodic structures. He is a reviewer for many EM journals.

Alessandro Fanti (Member, IEEE) received the Laurea degree in electronic engineering and the Ph.D. degree in electronic engineering and computer science from the University of Cagliari, Cagliari, Italy, in 2006 and 2012, respectively. From 2013 to 2016, he was a Postdoctoral Fellow with the Electromagnetic Group, University of Cagliari, where he is currently an Assistant Professor. His research interests include the use of numerical techniques for modes computation of guiding structures, optimization techniques, analysis and design of waveguide slot arrays, analysis and design of patch antennas, radio propagation in urban environment, modeling of bio-electromagnetic phenomena, microwave exposure systems for biotechnology and bio-agriculture. He is an Associate Editor for the IEEE JOURNAL OF ELECTROMAGNETICS, RF AND MICROWAVES IN MEDICINE AND BIOLOGY (J-ERM). From 2020 to 2023, he acts as Principal Investigator of the IAPC project, funded with five million euros by the Italian Ministry of Economic Development (MISE), within the AGRIFOOD PON I&C 2014-2020 (CUP: B21B1900064008 COR: 1406652).